EXPERIMENTAL NEUROLOGY **153,** 8–22 (1998)
ARTICLE NO. EN986852

Multivariate Analysis of Laminar Patterns of Neurodegeneration in Posterior Cingulate Cortex in Alzheimer's Disease

Brent A. Vogt, Leslie J. Vogt, Kent E. Vrana, Lynda Gioia, Robert S. Meadows, Venkat R. Challa, Patrick R. Hof,* and Gary W. Van Hoesen†

*Cingulum NeuroSciences Institute, 101 North Chestnut Street, Winston-Salem, North Carolina 27101, and Department of Physiology and Pharmacology, Wake Forest University School of Medicine, Medical Center Boulevard, Winston-Salem, North Carolina 27157-1083; *Neurobiology of Aging Laboratories, Fishberg Research Center for Neurobiology, Department of Geriatrics and Adult Development, and Department of Ophthalmology, Mount Sinai School of Medicine, One Gustave L. Levy Place, New York, New York 10029-6574; and †Department of Anatomy, University of Iowa, Iowa City, Iowa 52242*

Received September 22, 1997; accepted May 9, 1998

Posterior cingulate cortex is the site of earliest reductions in glucose metabolism and qualitatively different laminar patterns of neurodegeneration in Alzheimer's disease (AD). This study used multivariate analyses of area 23 in 72 cases of definite AD to assess relationships between laminar patterns of neurodegeneration, neurofibrillary tangle (NFT) and senile plaque (SP) densities, age of disease onset and duration, and apolipoprotein E (ApoE) genotype. No age-related changes in neurons occurred over four decades in 17 controls and regression analysis of all AD cases showed no relationships between neuron, SP, and tau-immunoreactive NFT densities. Principal components analysis of neurons in layers III–Va and eigenvector projections showed five subgroups. The subgroups were independent because each had a full range of disease durations and qualitatively different laminar patterns in degeneration suggested disease subtypes (ST). Cases with most severe neuron losses (STSevere) had an early onset, most SP, and highest proportion of ApoE ϵ4 homozygotes. Changes in the distribution of NFT were similar over disease course in two subtypes and NFT did not account for most neurodegeneration. In STII–V with moderate neuron loss in most layers, cases with no NFT had a disease duration of 3.5 ± 0.9 years (mean ± SEM), those with most in layers IIIc or Va had a duration of 7.3 ± 1 years, and those with most in layers II–IIIab had a duration of 12.1 ± 1 years. In STSevere, cases with highest NFT densities in layers II–IIIab also were late stage. Finally, ϵ4 homozygotes were most frequent in STSevere, but four statistical tests showed that this risk is not directly involved in neurodegeneration. In conclusion, multivariate pattern recognition shows that AD is composed of independent neuropathological subtypes and NFT in area 23 do not account for most neuron losses. © 1998 Academic Press

Key Words: **neocortex; senile plaques; tau immunohistochemistry; apolipoprotein E genotype; eigenvector projections.**

INTRODUCTION

Heterogeneity of functional impairments in Alzheimer's disease (AD) is well documented. Disease onset before the age of 65 years is associated with more severe language dysfunction (18), disruption of cholinergic (6, 73) and noradrenergic (8) systems, and neurodegeneration (51) than in late-onset cases. Early-onset disease itself is not uniform because there are two genetic defects (amyloid precursor protein and presenilin mutations; 30, 91) and a risk factor (apolipoprotein E (ApoE)-ϵ4 homozygotes; 7) associated with these cases. Heterogeneity also occurs as subgroups of patients with semantic or spatial impairments, yet at similar levels of impaired memory and intellectual abilities (52, 53). Cortical glucose metabolism suggests four subgroups of AD (27) with focal hypometabolism related to impaired visuospatial, language, or behavioral functions (22, 31). Such heterogeneities are either subgroups reflecting stochastic expression of a single process or subtypes resulting from multiple etiologies.

One argument for subtypes is posterior cortical atrophy in AD and a Bálint syndrome-like presentation. This syndrome includes paralysis of visual fixation associated with optic ataxia and a disturbance of visual attention that were first associated with bilateral parietal lobe lesions by Bálint (3, 29, 59, 20). In addition, variable disturbances in visual function include alexia, anomia, agraphia, and transcortical sensory aphasia with relatively good preservation of memory in the early stages of the illness (21, 46, 47, 63). Posterior cortical atrophy has been observed with imaging modalities and is associated with impairments in functional subsystems associated with visual processing in occipital, posterior parietal and cingulate cortices, and caudal temporal cortex (5, 37, 38, 40, 41, 70, 81, 86, 90). The focal atrophy is associated with NFT in layer V of secondary visual areas that are involved in motion detection and eye movement and posterior cingulate

0014-4886/98 $25.00

cortex (PCC) which is involved in visuospatial processing (66). No focal atrophy, fewer NFT, and neuron densities occur in frontal cortex (37, 38, 41, 86).

Although multifocal cortical atrophies with functional subsystem impairments and unique clinical endpoints support the subtype hypothesis (86), there have been few attempts to devise a methodology for postmortem assessments of the structural bases for subtypes. In addition to the transmitter system studies that emphasize bimodal effects of subcortical alterations cited above, multivariate methods have been used to identify five subtypes based on SP, NFT, atrophy, and other measures of pathology (1). Relationships among SP and NFT in subtypes are not yet clearly defined. There is no relationship between SP and clinical course in biopsy (4, 50) and postmortem (2, 42) tissue, SP are not related to dementia severity (62, 64) and neurodegeneration (77, 89), and there are instances of many SP in elderly individuals with preserved mental status (9, 15, 36, 44, 75, 76). Although NFT are related to disease duration (62), functional impairment correlated with NFT in medial temporal structures (2, 43), and dementia severity (62, 64), no relationship between neuron losses and progression occurs in biopsied and autopsied neocortex (4, 50).

It is well known that large cortical neurons degenerate (77) and can form NFT (38, 69). Neuron loss is correlated with psychological performance in AD (64) and the extent of neuron loss is related to disease duration (43) and age at death (51). A combined biopsy and autopsy study showed a significant relationship between disease progression and the loss of cortical neurons (50). Studies that seek to define neurodegeneration for the entire neocortex, however, meet a number of problems: (i) Cases with multifocal atrophy which do not have uniform loss of neurons throughout neocortex cannot be included in samples that hypothesize uniform degeneration. (ii) In order to accommodate widely varying cytoarchitectures, these studies employ quartile depth measurements (77), emphasize two layers (60), or do not consider lamination (12). Each solution to defining a single pattern of neuron losses overlooks medium-sized pyramids and averages across many areas.

A solution to the problems of averaging, multifocal atrophy, and variations in disease progression is to focus on a single area and consider neuron densities in terms of the unique cytoarchitecture and full disease course. We have done this with PCC (89) and it is possible that the different laminar patterns of cell loss observed are associated with different mechanisms and represent neuropathological subtypes within AD (86). For example, degeneration of neurons mainly in layer IIIab may require a different mechanism from that of degeneration of neurons mainly in layers IV and V. Changes in receptor binding support unique mechanisms (82, 83). Thus, laminar patterns in vulnerability result from structural, connectional, and neurochemical differences among neurons.

The PCC is involved in AD including alterations in neurochemistry (71, 72), glucose metabolism (27, 34, 57), neurodegeneration (12, 60), and SP and NFT formation (11). Glucose hypometabolism occurs in PCC very early in the disease and is more severe than in lateral neocortex and medial temporal structures in cases that present first with memory impairments (58). In addition, PCC is involved in visuospatial and memory processing (66, 67, 78) and has abundant connections with parahippocampal and parietal cortices (88), suggesting that functional impairments previously attributed to other regions may be a consequence of impaired function in PCC. Therefore, we tested the subtypes hypothesis by analyzing neurons, SP, and NFT in PCC and ApoE genotype with a multivariate model. Tau immunohistochemistry and thioflavine S were used to assess NFT in a multivariate model for different layers. Neuron counts were made on two times the number of samples for each case and three times the number of cases were assessed as done previously (89).

MATERIALS AND METHODS

Case Material

The cases were derived from the Wake Forest University School of Medicine Brain/DNA Resource Center; the University of Iowa Deeded Bodies Program, the Division of Neuropsychiatry; University of Geneva, Switzerland; and the Harvard Brain Tissue Resource Center, McLean Hospital, Belmont, Massachusetts (PHS grant MH/NS31862). Control cases were neurologically intact individuals and the AD cases were diagnosed as definite AD (45, 56) at each of the above institutions before they were entered into the research protocol. In addition to the latter cortical criteria, all cases had above age-matched control numbers of NFT in entorhinal and perirhinal cortices and cases were excluded from the database based on the following observations: histories of significant drug abuse; evidence of strokes, multi-infarct dementia, Binswanger's disease, diffuse Lewy body disease, Parkinson's disease or signs of infection; and neuronal changes consistent with an acute terminal hypoxic ischemic episode. A total of 9 cases were excluded that had Lewy bodies in the substantia nigra according to consensus guidelines (55). No cases with Lewy bodies were included in the sample. Seven of the cases that were used for this and a previous study did not have microscopic assessments of the substantia nigra. However, removal of all 15 cases used from the earlier study (89) did not alter the statistical analysis of subtypes as discussed below and Lewy body disease has a normal density of cortical neurons (49).

In an elderly population there can be an occasional small infarct, moderate atheroarteriosclerosis, and mild to moderate cerebral amyloid angiopathy. Infarcts were overlooked only if they were infrequent (one or two per case), small (<2 mm diameter), and in regions that are not connected with PCC as assessed in monkey cortex (88). There were 72 cases with a definite diagnosis of AD and 17 neurologically intact and control cases for a total of 89 cases. The control and AD groups appear similar in some features including postmortem interval and brain weight. As is typical for healthy controls, this group experienced little pneumonia and infection but proportionately more deaths from cancer. Although the age at death appears lower in the control than most AD subgroups, the age at death for all AD cases was 79 ± 1.1 years and did not differ from the control group. Case information is also summarized in Table 1 according to subgroups as discussed throughout the text. Most subgroups had similar profiles like death by pneumonia and cardiopulmonary arrest. The only AD subgroup that had a unique profile was the subgroup with severe degeneration with earlier death (74 ± 2.8 years), age of onset (Table 2), and lower brain weight (1050 ± 52 g). Other differences, like a high proportion of males in ST0, are attributed to small sample size.

Fifteen AD cases used previously (89) were used here because tissue was available for genotyping and 6 of the control cases were used from the earlier study. Although there were no selection criteria imposed that would alter the PCA, we performed the analysis with and without these 15 cases to determine whether or not the new set of 57 cases provided an independent verification of earlier observations. The variance and associated percentage of the total for each principal component (PC) were as follows for all 72 cases: PC1, 283406/96.4%; PC2, 7275/2.5%; PC3, 2308/0.79%. Removal of the 15 previous cases did not alter the five subtypes; i.e., there was no overlap of individual cases among subtypes in the eigenvector projections. Furthermore, the variance for each PC and the loading factors for each layer were not changed. The variance and associated percentage for each PC for the new 57 cases were as follows: PC1, 211245/96.6%; PC2, 5156/2.4%; PC3, 1627/0.74%. The new 57 AD cases provide critical validation of previous findings (89).

Tissue Preparation and Quantification

Formalin-fixed blocks from five cortical regions were used: PCC, prefrontal areas 10 and 46, inferior parietal area 40, and temporal area 20/entorhinal cortex/hippocampus. The blocks were cut into six series of sections at a 50 μm thickness and four series of 100 μm thickness on a sliding microtome. A series was stained with thionin or thioflavine S as described previously (89). The thioflavine S protocol labels both diffuse and neuritic plaques and no distinction was made between these when reporting SPs. Four to six sections from another series were immunoreacted for tau with an anti-tau antibody (mouse monoclonal antibody AD2 at 1:1000 dilution; 13), biotinylated horse anti-mouse antiserum, ABC solution, and diaminobenzidine. Each cortical region was drawn at 17× from the Nissl-stained sections and used to interpret the thioflavine S-stained preparations. A qualitative survey of an entire gyrus was made before determining the representative density of SP or NFT. A 400 × 400-μm grid was used to count SP and NFT densities by layer in 0.32 mm^2. The counts for SP were summed for all layers to give an overall density for 1.92 mm^2. The average density of SP for all AD cases was 30.3 ± 1.93 and our threshold for comparison with age-matched control cases was 20 SP. This was an internal standard to assure that all cases had AD.

Neuron counting was performed on the thionin-stained sections as discussed previously (89). The perikarya of neurons only were drawn in 160-μm-wide strips of area 23a with a drawing tube attached to the

TABLE 1

Characteristics of Cases

	n	Age at death (mean ± SEM)	Gender (M/F)	PMI	Brain weight (g)	Causes of death						
						Pneu	CPA	Sep	Can	DH	RF	NA
Controls	17	74 ± 2.9	8/9	7.8 ± 1.9	1213 ± 34g	1	7	—	7	—	—	2
All AD	72	79 ± 1.1	34/38	6.1 ± .75	1118 ± 20	24	19	5	1	7	2	14
ST0	5	79 ± 5.1	4/1	7.7 ± 4.4	1222 ± 23	2	2	1	—	—	—	—
STIIIab	7	77 ± 4.3	4/3	5.7 ± 1.3	1102 ± 75	3	—	—	—	2	—	2
STIV–V	13	81 ± 2.2	6/7	8.2 ± 2.6	1171 ± 45	5	3	—	—	1	—	4
STII–V	30	82 ± 1.4	13/17	6.4 ± 1.3	1145 ± 28	10	9	3	1	2	1	4
STSevere	17	74 ± 2.8	7/10	6.0 ± 1.2	1050 ± 52	4	5	1	—	2	1	4

Note. PMI, postmortom interval; Pneu, pneumonia; CPA, cardiopulmonary arrest; Sep, sepsis; Can, cancer; DH, dehydration; RF, renal failure; NA, not available.

TABLE 2

Laminar Area and Neuron Atrophy Correction

A. Laminar area in mm^2 (mean ± SEM)

	Layer IIIab	Layer IIIc	Layer IV	Layer Va
Control	0.0604 ± 1.96	0.0642 ± 2.29	0.0453 ± 1.77	0.0390 ± 1.92
ST0	0.0606 ± 3.30	0.0625 ± 4.18	0.0450 ± 3.61	0.0385 ± 4.68
STIIIab	0.0341 ± 1.84*	0.0601 ± 2.41	0.0414 ± 1.00	0.0331 ± 0.75
STIV–V	0.0522 ± 2.16	0.0594 ± 2.35	0.0398 ± 1.46	0.0303 ± 1.00*
STII–V	0.0434 ± 1.34*	0.0521 ± 1.53*	0.0370 ± 1.21*	0.0277 ± 0.67*
STSevere	0.0361 ± 2.17*	0.0462 ± 2.02*	0.0357 ± 1.18*	0.0237 ± 0.91*

* Layers with greatest atrophy versus control values ($P < 0.001$).

B. Laminar area as a percentage difference from control

ST0	0	−2.6%	0	0
STIIIab	−43.5%	−6.4%	−8.6%	−15.1%
STIV–V	−13.6%	−7.5%	−12.1%	−22.3%
STII–V	−28.1%	−17.9%	−18.3%	−29.0%
STSevere	−40.2%	−28.0%	−21.2%	−39.2%

C. Neuron atrophy correction (neurons/mm^2)

	Layer IIIab	Layer IV
ST0	949.8 ± 35.97	1190.5 ± 114.81
STIIIab	915.7 ± 72.79	934.2 ± 101.51
STIV–V	1028.6 ± 36.58	570.5 ± 41.49
STII–V	738.9 ± 38.55	506.5 ± 33.32
STSevere	453.9 ± 32.92	151.3 ± 14.39

microscope. The cytoarchitectural characteristics of area 23a have been described (87). In order to reduce the variance among individual counts for each case, six strips were drawn from each case (two from each of three slides) and the mean neuron number was calculated for each layer. Neurons were only included in the count that had a nucleus and nucleolus. Glia were excluded during the drawing process and were usually less than 8 μm in diameter, had pale-staining nuclei, and had limited and poorly stained cytoplasm. These drawings were used to locate tau-immunoreactive NFT. The sections were aligned by area and layer and each NFT was plotted with the drawing tube and an average number of NFT per layer was calculated for two to four sections from each case. Samples of area 23a were chosen at suprasplenial levels. Since the sampling technique is critical for localizing the same area in each case, we assessed the extent to which neuron densities varied in the rostrocaudal extent of this area. In five cases neurons were counted from coronal levels of area 23a that were 3–3.5 mm apart. There were no differences in neuron counts for any layers in anterior or posterior parts of area 23a. There were also no differences in densities between control cases under or over the age of 65 years or by gender.

Neuron numbers for each layer were not atrophy corrected. The decision not to correct for atrophy is fundamental to identifying subtypes with the multivariate model and Table 2 shows the actual area in each layer in which neuron counts were made. The effects of atrophy correction are shown for a layer that undergoes significant atrophy (layer IIIab) and one that undergoes less atrophy (layer IV). The correction in layer IIIab normalizes neuron density in three subtypes including STIIIab. In layer IIIab of STIIIab, there is a 43.5% reduction in area and a 54% reduction in neurons (Table 3). Each of these changes cancel for no net change in neuron density when compared to ST0 and STIV–V (Table 2C), yet it is clear that layer IIIab is devastated in STIIIab. Layer IV undergoes less atrophy and, since there are reductions in neuron counts, the atrophy correction replicates these changes. Hense, atrophy correction can produce misleading information about the number of neurons in a layer when there is atrophy. The rationale for atrophy correcting neuron data is not straightforward and is considered further in the discussion. Samples from unfixed and formaldehyde fixed cases were genotyped to determine the allelic composition for each individual according to the technique of Gioia *et al.* (24).

TABLE 3

Properties of Subtypes Based on Neurodegeneration

Neurons	Controls $n = 17$	ST0 $n = 5$	STIIIab $n = 7$	STIV–V $n = 13$	STII–V $n = 30$	STSevere $n = 17$
IIIab	68 ± 3	58 ± 5	***31 ± 3***	54 ± 2	***33 ± 2***	***17 ± 2***
IIIc	61 ± 3	60 ± 3	51 ± 4	46 ± 2	***34 ± 1***	***22 ± 2***
IV	54 ± 3	52 ± 3	39 ± 4	***25 ± 3***	***19 ± 1***	***6 ± 1***
Va	48 ± 4	44 ± 4	33 ± 2	***29 ± 1***	***20 ± 1***	***8 ± 1***
Total	231 ± 11	***214 ± 13***	***155 ± 13***	***154 ± 3***	***107 ± 4***	***53 ± 4***
Duration (years)	NR	1–10	3–15	2–10	1–14	4–25**
Onset (years)	NR	73 ± 6	69 ± 5	75 ± 2	74 ± 1	63 ± 3
SP*1	8 ± 3	16 ± 3	32 ± 2	22 ± 5	28 ± 2	39 ± 4
NFT*2	0.1	27 ± 14	39 ± 15	2 ± 1	20 ± 5	43 ± 8
NFT*3	0	0	24 ± 3	10 ± 4	25 ± 4	30 ± 6
ϵ4/4%	NA	20	29	15	20	42

Note. Mean ± SEM. Bold and italicized numbers differ significantly ($P \leq 0.05$; protected t tests) from controls. Double underlines identify STSevere properties in the lower half of the table and single underlines are for subtypes that differ significantly from this subtype ($P \leq 0.05$; protected t tests). NR, not relevant. *1, thioflavine S-stained SP; *2, thioflavine S-stained NFT; *3, tau-immunoreactive NFT—two cases in ST0 had no tau-ir NFT. ** Ranges for each subtype. NA, not assessed.

Statistical Analyses

The hypothesis was first tested that AD is uniform and differences among cases were due to disease progression and assessed with linear regression analysis. Values for F with a $P \leq 0.05$ were accepted as significant and t tests protected for multiple comparisons for all control versus all AD cases as a group. However, evidence supported the hypothesis that AD was not uniform and principal components analysis (PCA) and pattern recognition in eigenvector projections was applied to assess neurons and other measures of the disease that might account for statistical subgroups and/or subtypes. The Ein*Sight statistical and pattern recognition software (InfoMetrix, Woodinville, WA) was used for this purpose and is a noniterative partial least squares method for computing the principal components or eigenvector for each point in a multivariate analysis. This approach incorporates multiple variables including normalization and scaling of variables to remove bias arising from differences in magnitude so that each variable has equal weight. An eigenvector is calculated for each individual and a three-dimensional eigenvector projection created where the distance from the origin is proportional to the importance of a variable in the principal component loading of that variable; points close to the origin have limited information, whereas a large distance from the origin has a high loading and means that the variable is important to the analysis. Rotation of the eigenvector projection for pattern recognition allows one to investigate clustering and the influence of outliers on a subgroup. The mutual location of individuals in the eigenvector projection reflects their coherence and membership in a subset with unique properties.

RESULTS

Neurons Over Four Decades of Normal Aging

The 17 control cases were evaluated for the extent to which aging involves neurodegeneration in area 23. In addition, the possible effects of sampling from different rostrocaudal levels of this region and gender were assessed. The controls had an age at the time of death of 74 ± 2.9 years (mean ± SEM) and a range of 56–94 years. Linear regression analyses of neurons in each layer as a function of age at death showed no significant correlation coefficients. For example, layers IIIc and Va have the largest neurons in area 23a and the correlation coefficients and associated F and P values for these layers were as follows: IIIc, $r = -0.13$, $F = 0.29$, $P = 0.6$; Va, $r = 0.12$, $F = 0.22$, $P = 0.65$. Thus, age-related neurodegeneration could not be detected in PCC over four decades of normal aging. Neurons in 5 cases for which all of PCC was available were calculated for each layer in area 23a at two rostrocaudal levels: dorsal to the caudal end of the splenium of the corpus callosum and 3–3.5 cm rostral to this level. There were no differences among neurons as exemplified in the following layers (anterior/posterior levels): IIIab, 62 ± 3.7/68 ± 5.2; IIIc, 61 ± 3.5/62 ± 5.9; IV, 62 ± 4.4/66 ± 4.3; Va, 42 ± 2.8/54 ± 4.5. Finally, there were no gender differences in the neurons in midcortical layers (female/male): IIIab, 70 ± 3.9/66 ± 4.6; IIIc, 60 ± 3.1/62 ± 4.4; IV, 58 ± 4.7/52 ± 4.6; Va, 50 ± 2.6/48 ± 3.3.

Alzheimer's Disease Group Analysis

The null hypothesis states that there are no subtypes within AD and that differences in neurons, NFT, and SP can be accounted for by differences in disease

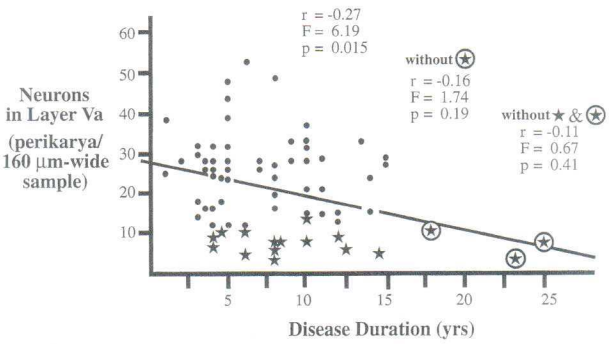

FIG. 1. Multiple regression analysis of neurons in layer Va along clinical disease duration for all AD cases. Although the F value of 6.19 was significant, this is due solely to three outliers (circled stars) that are members of a subgroup of cases with severe neurodegeneration in all layers. Removal of these outliers reduced the F to a nonsignificant 1.74 and removing cases with severe degeneration (stars) reduced the F ratio further (0.67).

duration for a uniform disease. The 70 AD cases with a retrospective estimate of disease onset in at least one cognitive domain were assessed as a group in relation to disease duration, age at death, and age at disease onset. Since large neurons form NFT and degenerate in AD, and these neurons are mainly in layers IIIc and Va in PCC, these layers were used to assess neurons over the disease course. Neurons were not related to age at death or age at disease onset for either layer, but there were relationships between neurons in both layers and disease duration. Figure 1 shows layer Va neurons for all AD cases plotted against disease duration ($n = 70$; $r = -0.27$; $F = 6.19$; $P = 0.015$). Three cases, however, stood out as outliers with durations of 18–25 years. Removal of these cases reduced the F statistic to 1.74 ($P = 0.19$). Furthermore, these outliers were members of a subgroup with severe degeneration in all layers (stars in Fig. 1) and their removal from the analysis produced an F of 0.67 ($P = 0.41$). The same effect was observed for layer IIIc. The dramatic outlier effect on the regression analysis suggests that there was no relationship between neurons and disease duration and the subgroup with severe neurodegeneration is a unique subtype with a full range of disease durations. The extent to which NFT are related to disease duration and neurodegeneration was assessed in layers III and V, since there were more thioflavine S-stained NFT in these than other layers when at least one NFT was present (II = 5 ± 0.97; III = 8 ± 1.3; IV = 3.6 ± 0.49; V = 15 ± 2; VI = 3.6 ± 0.7). There were 21 cases with no thioflavine S-stained NFT and there were no correlations between neuron and NFT nor NFT and disease duration.

Laminar Patterns of Neurodegeneration

The hypothesis of independent classes of AD has been proposed for PCC (89). Neurons in each layer of each case were compared sequentially (i.e., one layer at a time) with average control values to determine which layers had the greatest proportionate neuron loss. Since a methodology was needed to include multiple layers in a single statistical model, neurons were assessed in layers IIIab, IIIc, IV, and Va for PCA and eigenvector projection (Fig. 2A). There was no overlap between these groups except for 5 AD cases with neuron counts similar to controls. The AD cases were then plotted without controls so that the full variance and covariance in the AD group could be represented in the eigenvector projection (Fig. 2B) and cases color coded according to five patterns of neurodegeneration. The three-dimensional graph was rotated so that segregation of the groups could be best visualized. Five laminar patterns were defined as previously done (89) and the following subtypes (ST) defined: ST0, no apparent loss; STIIIab, neuron losses mainly in layer IIIab; STIV–V, losses mainly in layers IV and/or V; STII–V, losses of 35–70% throughout most layers; STSevere, losses over 80% in most layers. Although the STII–V includes significant loss of neurons in many layers, even here there were laminar preferences for neurodegeneration. In 22 of 30 cases the greatest loss was in layer IV and this could reach 80% ($n = 4$). The average loss in layer IV for all 22 cases was 71 ± 2% with the second greatest percentage loss occurring in layer Va or Vb (−58 ± 4%). This subgroup, however, cannot be equated to STIV–V because in STII–V there is substantial degeneration in superficial layers. For example, in the 19 cases with greatest superficial losses in layer IIIab there was a reduction of 53 ± 2.4%. Finally, two cases were not included in this PCA because they were outliers in preliminary PCA: one each in STIV–V and STII–V.

Although neurons in layers III–Va were used because they were previously used to define classes (89), the PCA can be used to assess other layers. For example, including layer II for subgroups that differ from controls (i.e., excluding ST0) produced an eigenvector projection with reduced subgroup definition because of case overlap at the border of STIV–V and STII–V. In addition, layers Vb and VI were not part of the analysis because layer Vb is neuron sparse and layer VI is variable in thickness at the ventral apex of the cingulate gyrus and has variable neurons due to cortical convolutions.

The null hypothesis requires etiological uniformity, a single continuum of neurodegeneration, and differences due only to disease duration. It was rejected for the following reasons. First, linear regression analysis of neurons against disease duration for each subtype showed no significant losses of neurons in any layer, precluding an interaction among subtypes. Second, each subtype has a full range of disease durations

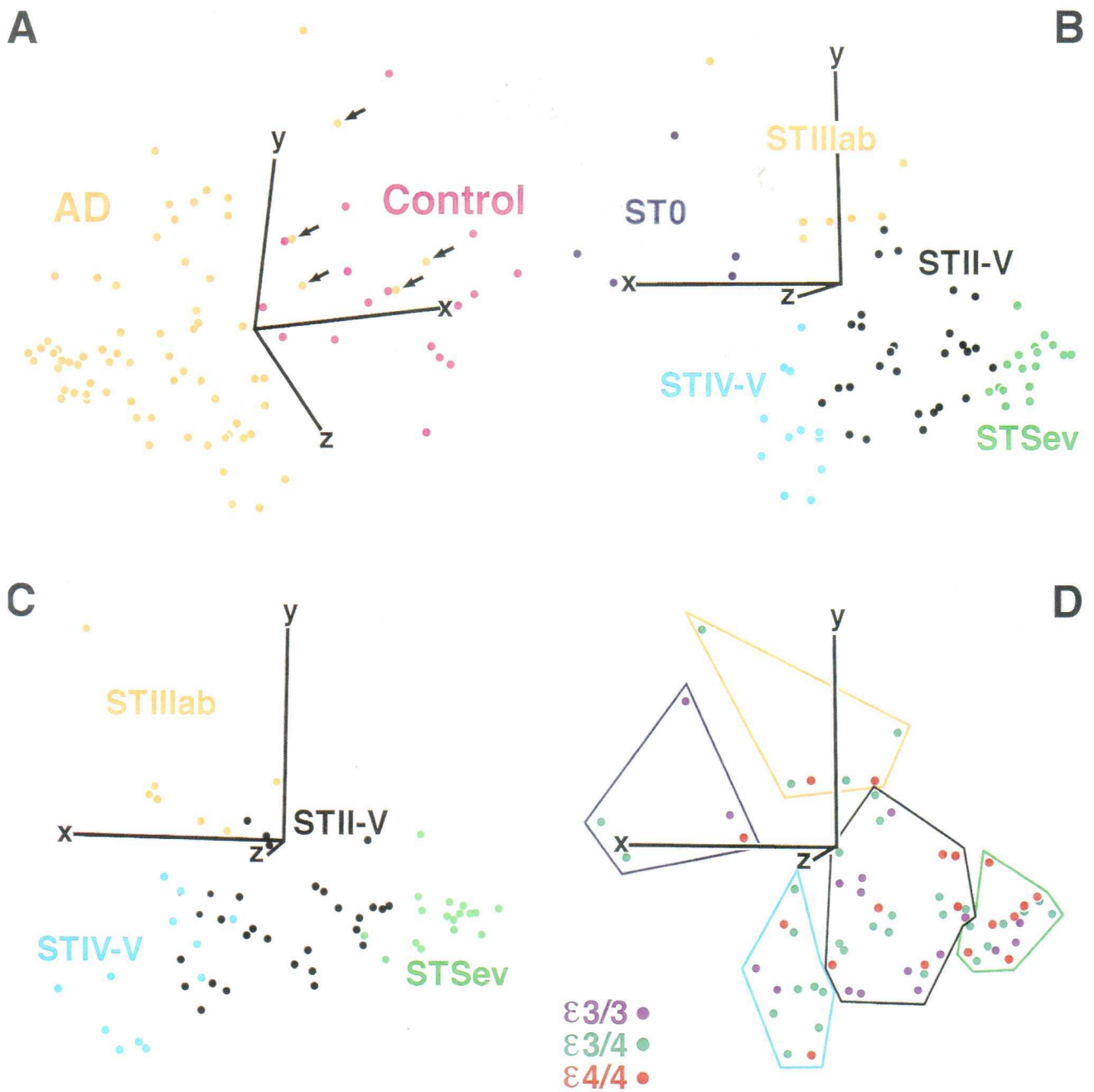

FIG. 2. Eigenvector projections of PC scores of neurons in layers IIIab, IIIc, IV, and Va. Graphs were rotated to demonstrate optimally the statistical subgroupings. (A) All AD (orange) and control (purple) cases; the five AD cases that overlap with the controls (arrows) had neuron counts like controls. (B) Each subtype is color coded according to layer-by-layer analysis of neurons vs control cases which produced five subgroups: ST0 (purple), STIIIab (orange), STIV–V (blue), STII–V (black), STSevere (STSev, green). (C) Layer II was added to determine if it provided greater subgroup segregation. Since there was no improvement and the STIV–V/STII–V border was blurred, the multivariate model need not include neurons in this layer. (D) A test that ApoE genotype has a specific role in neuron losses is adding and ApoE risk score for each case and color code the data according to genotype as shown. There was no evidence for subgrouping by genotype except in STSevere.

(Table 3). Since most severe neuron losses were associated with the youngest individuals, there was little chance that layer-specific neuron losses in subtypes with late onset lead to severe neurodegeneration in early-onset cases. Also, if the subtypes were a simple continuum, disease duration should lengthen from ST0 to STSevere and it does not. Third, the PCA shows unique values for each individual in a subtype and no overlap with other subtypes as would occur if there was a single continuum of cases.

Tau-Immunoreactive Neurofibrillary Tangles

Forty-eight cases were immunoreacted with the AD2 tau antibody (13) to assess neurofibrillary changes that are earlier in the disease than those apparent with thioflavine S (80). There were only 2–4 immunoreacted cases for ST0, STIIIab, and STIV–V and the density of tau-immunoreactive (ir) NFT was low and homogeneous across layers. The density of NFT in traverses of all layers for each subtype are provided in Table 3 (NFT*3). In STII–V, tau-ir sections were available for 23 of 30 cases, while 12 of 17 were tau-ir in STSevere. The STII-V cases could be grouped according the layer of highest NFTs: (i) none, $n = 4$; (ii) highest in layers IIIab or Va, $n = 13$; (iii) highest in layer II, $n = 4$. Two cases had a low density and even distribution and were not included in these subgroups. Disease duration was directly related to these three groups: (i) no NFT = 3.5 ± 0.9 years; (ii) layers IIIab or Va = 7.3 ± 1 years; (iii) layer II = 12.1 ± 1.0 years. Thus, disease progression was associated with hyperphosphorylation of tau in layers IIIab and V first and later in layer II. Tau phosphorylation in layer II marks the latest stage of STII–V progression. Neuron counts in layers II–Va were not different among these groups.

A better test of relationships between disease duration and tau-ir NFT is PCA. The PC scores were derived with disease duration and NFT density for layers II–IIIab, IIIc–Va, and Vb–VI. These layers were used to account for shifts in the densities of NFT over the cortical layers at different stages of the disease. Figure 3A shows an eigenvector projection for STII–V and there are three subgroups identified by disease durations. A similar eigenvector projection occurred with STSevere; however, the second 3-D graph in Fig. 3B includes both subtypes because the disease duration relationship is not subtype dependent and statistical power is improved for the larger sample.

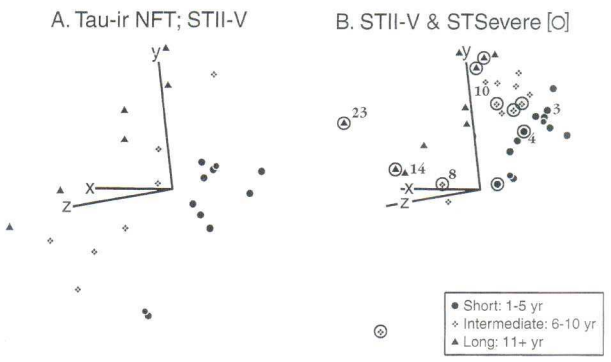

FIG. 3. Eigenvector projections for STII–V (A) and STII–V/STSevere (individual cases circled) together (B). The multivariate model included disease duration, tau-ir NFT in layers II–IIIab, IIIc–Va, and Vb–VI. In both instances three subgroups are apparent confirming that NFT densities and their laminar distribution are related to disease progression. Although a similar phenomenon was apparent for STSevere alone, the cases were combined in B to provide stronger statistics. The laminar distribution of NFT is related to disease progression not subtype per se. The numbers in this figure refer to the cases by disease duration shown in the next figure (note: 4 here is equal to 4.5 in Fig. 4).

The stages of NFT deposition can be quantified for STSevere, as above for STII–V, and examples are photographed for each (Fig. 4). Tau-ir NFT in STSevere showed either a low density and even laminar distribution ($n = 3$, 9.4 ± 1.2 year duration) or high density in layers V, III, and VI or layers II–IIIab ($n = 8$, 8.5 ± 1.5 year duration). Layer V appeared to be the earliest in which tau phosphorylation occurred and layer III was next. Layers II–IIIab were the last to contain tau-ir neurons and had lowest overall density of neuropil threads. In addition, NFT in layer V may disappear in late stages of the disease (Fig. 4; 23 year case). However, neurodegeneration was not associated with differences in tau-ir NFT as was true for STII–V. This was true for total neurons in layers IIIab–Va (onset <5-year duration = 58 ± 8.9 neurons; cases 8+ years = 54 ± 4.6) and neurons in layer IIIab (<5-year duration = 20 ± 2.9 neurons; 8+ years = 18 ± 1.8). Finally, there were more thioflavine S-stained SP in cases with high densities of tau-ir NFT (47 ± 4.7) than there were in cases with few such NFT (26 ± 2). Cases with a high density of tau-ir NFT in layers II and/or IIIab had a high density of thioflavine S-stained NFT. Thus, the density and laminar patterns of tau-ir NFT are related to disease progression in STII-V and STSevere, they do not undergo obligatory formation of β-pleated sheets, their presence in layer II is a marker of terminal disease, and NFT in layer V may be removed from the neuropil in end-stage cases.

Neurofibrillary Tangle and Neuron Relationships

The hypothesis that insoluble NFT serve as a mechanism of cell death requires a direct test. Cases from STII–V were used because of the large number of cases that were tau-ir and the broad laminar pattern of neurodegeneration. Linear regression was performed on NFT coregistered to perikaryal samples of neurons for layers II, III, IV, and Va, each separately. There were no significant correlations in these data for layers II, IV, or Va but there was a strong, inverse relationship in layer III ($r = -0.65$; $F = 17$; $P = 0.0001$). This relationship could be misleading because there may not be a 1:1 ratio of NFT:neuron loss. This was assessed by calculating the number of neurons lost in layer III in each case as a difference of neurons in layer III from the average for the control group (average of 129 neurons). Four cases with no tau-ir NFT had lost 52 ± 1.6 neurons in layer III, whereas two cases had high NFT densities of 22 and 31 and neuron losses of about 80. Excluding these six extreme cases, NFT were 3–18 and neuron losses were 45–87. The ratio of NFT:neuron loss for each case was calculated for the same area of layer

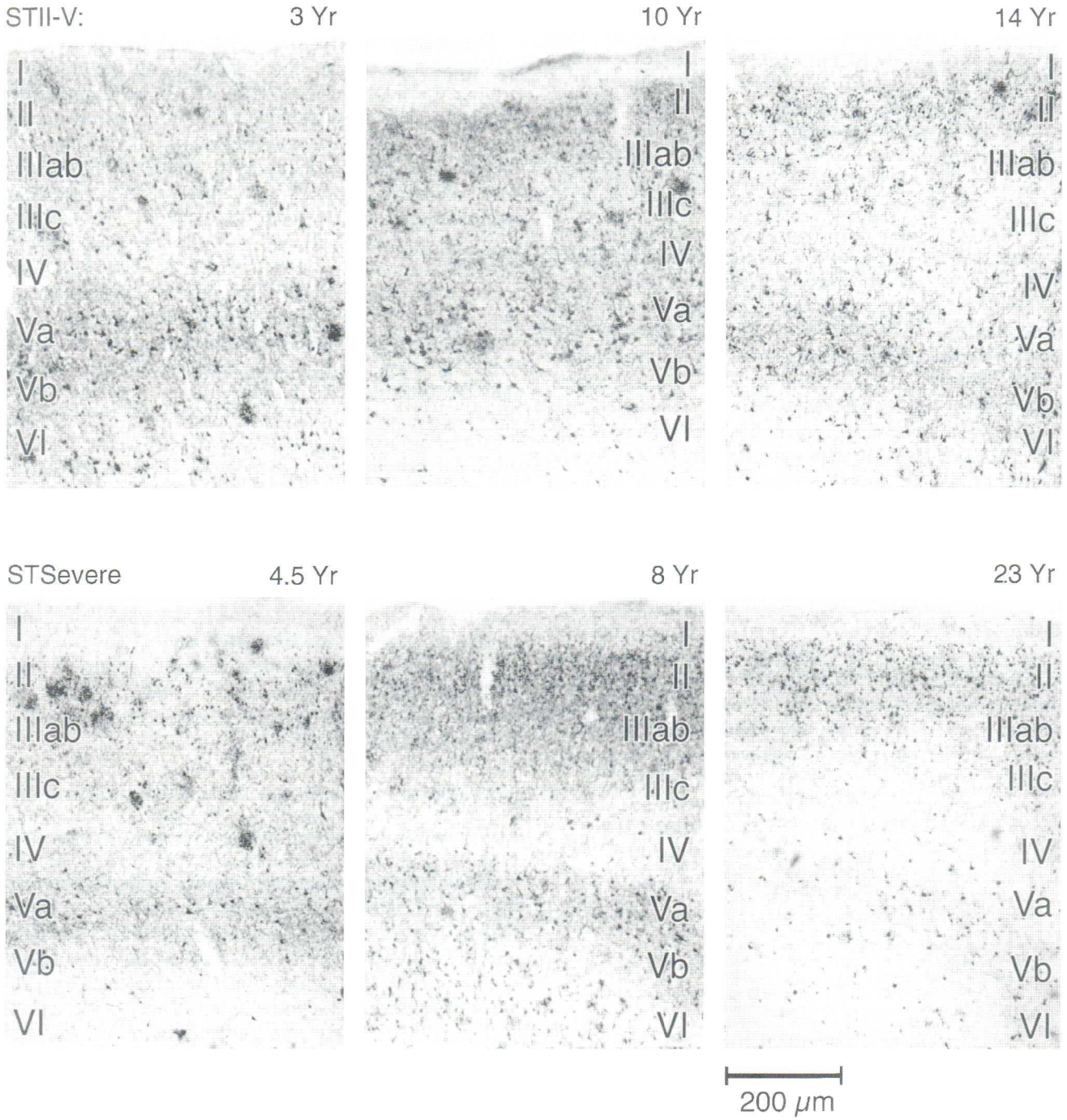

FIG. 4. Tau immunohistochemistry for individual cases from two subtypes. (STII–V) Cases with 3 or fewer years duration usually had no tau-ir NFT and some had NFT mainly in layer Va as shown in the first case. The second case had a higher density of NFT in both layers III and Va as well as an overall higher level of neuropil threads. The third case had a long duration and high level of tau-ir NFT in layers II and IIIab and relatively fewer in deeper layers. (STSevere) The shortest duration case available with tau-ir NFT (4.5 years) had approximately equal densities of tau-ir NFT in layers III and Va. There were more neuropil threads in intermediate stages of the disease (8 years). Although layer II had NFT in each of these cases, layers II and IIIab in the 23-year case were highest and there were few NFT in deeper layers.

III. The range of ratios was 3.4–22 and the mean ratio was 7.7 ± 1.0. Thus, an average of 8 neurons was lost for each NFT formed in layer III of STII–V. These relationships were analyzed with PCA and the following seven variables for each case: disease duration; NFT in layers III, IV, and Va; and neurons in layers III, IV, and Va. Disease duration (short, 1–5 years; intermediate, 6–10 years; long, 11 + years) did not identify three subgroups in an eigenvector projection, confirming the lack of a relationship. Thus, tau-ir NFT formation is related to disease duration in STII–V and STSevere; however, the density of NFT does not account for neurodegeneration nor their laminar patterns. Subtypes based on laminar patterns of neurodegeneration are not the result of NFT formation.

Apolipoprotein E Genotype

There were more thioflavine S-stained SP in area 23 in ApoE ϵ4 homozygotes than there were in ϵ3 homozygotes or individuals heterozygous with each allele. Although the difference between the ϵ4 and ϵ3 homozygotes was not significant when an average density of SP was calculated (ϵ4/4, 30 ± 3.2; ϵ3/3, 24 ± 5.4), they were significant when the maximum density of SP was used for the analysis (ϵ4/4, 31 ± 3; ϵ3/3, 22 ± 2; $P < 0.05$). The ϵ4 homozygotes were at a higher proportion only in STSevere, while the proportion of ϵ4 homozygotes was about the same in other subtypes (Table 3). Rank ordering of subtypes according to the proportion of ϵ4 homozygotes and age of disease onset for all cases in a subtype follows: STSevere, 42%/63 ± 3.4 years; STIIIab, 29%/69 ± 4.7; ST0, 20%/73 ± 5.8; STII-V, 20%/74 ± 1.4; STIV-V, 15%/75 ± 2.2. Differences between the age at onset for STSevere versus ST0, STIV–V, and STII-V were significant.

Although ApoE genotype in STSevere is associated with SP density and age of onset, it was not related to the density or distribution of tau-ir NFT. Classification of all cases regardless of neurodegeneration showed the following densities of tau-ir NFT: ϵ3/3 = 24 ± 6; ϵ3/4 = 28 ± 3.5; ϵ4/4 = 31 ± 8. A within-subtype analysis of the proportion of ϵ4 alleles to the total number of alleles showed the following for STII-V: no NFT, 4 of 12; NFT highest in layer IIIab or VI, 13 of 28; NFT highest in layer II, 3 of 6. In STSevere cases with low density and even laminar distribution of NFT, there were 7 of 12 ϵ4 alleles, while cases with highest NFT in layers II and/or IIIab had 6 of 14 ϵ4 alleles.

The high density of ϵ4 homozygotes in STSevere suggested that the ApoE risk factor could influence neurodegeneration; however, this is unlikely for the following reasons: First, although neurodegeneration in the other four subtypes was different (Table 3), the ϵ4 risk in these groups was about the same: 15–29%. Second, in STII–V there were enough ϵ4 ($n = 6$) and ϵ3 ($n = 7$) homozygotes to directly compare neurons for layers IIIab–Va; ϵ4 homozygotes had 98 ± 9 neurons and ϵ3 homozygotes had 116 ± 9, a nonsignificant difference. Third, PCA of groups based on the ApoE risk factor did not produce unique subgroups. Figure 2D shows a plot of eigenvalues for neurons in layers IIIab–Va coded for three groups: ϵ4 homozygotes; ϵ2 or ϵ3/ϵ4; ϵ2 or ϵ3/ϵ3. Rotation of the graph in all planes failed to uncover a subgrouping of any allelic combination including mainly ϵ4 homozygotes. Fourth, a measure of ApoE risk (ApoE risk score: 2 = ϵ2/3, 3 = ϵ3/3, 4 = ϵ2/4, 5 = ϵ3/4, 6 = ϵ4/4) with neuron counts in layers IIIab–Va failed to improve the multivariate model. Although the high density of ϵ4 homozygotes in STSevere is associated with severe neuron losses, early onset, and high amyloid levels, genotype is not specifically related to neurodegeneration.

DISCUSSION

Five laminar patterns of neurodegeneration were identified in AD with a multivariate model and eigenvector projections and each pattern was present early in the disease. Since multiple etiologies may be required to account for the five qualitatively different laminar patterns of cell loss, they are termed neuropathological subtypes and each is independent with a full range of disease durations. Although there is progressive tau phosphorylation beginning in layers IIIc–Va and culminating in layers II–IIIab at late stages, NFT formation does not account for most neurodegeneration nor subtypes. The STSevere is of particular interest because it has essentially no laminar architecture and is distinguished from other subtypes by its early onset, high deposition of SP, and high proportion of ApoE ϵ4 homozygotes. Although there is an association of ϵ4 homozygotes and high levels of amyloid, there was no specific association with laminar patterns of neurodegeneration and ApoE risk. These observations do not support the hypothesis that AD is a single disease based on global changes in one transmitter system, protein, or lipid metabolic impairment and studies that overlook PCC may miss early impairments in the structure and function of cortical cells.

Posterior Cingulate Cortex: A Site of Early Functional Lesions

Neurochemical, morphometric, and glucose metabolic studies implicate PCC in AD. Although early impairments in memory and visuospatial functions are often thought to result from disruption of medial temporal and parietal cortices, respectively, PCC itself is engaged in both of these functions (34, 66, 67, 78) and it is unclear to what extent each structure contributes to such functions. In addition, clinical assessments of AD emphasize memory impairments and can overlook early disturbances in vision, language, and behavior. Since

there are no neuropsychological tests to pinpoint functional disruption of PCC and it tends to be overlooked in postmortem assessments, the role of this region in early stages of AD is not appreciated. Recent functional imaging studies provide a direct methodology for analyzing impaired function throughout the cerebral cortex in AD and highlight the pivotal role of PCC.

Minoshima *et al.* (57, 58) reported that PCC is glucose hypometabolic in very early stages of AD in cases that first present with memory impairment. These data also show that PCC hypometabolism precedes that in medial temporal and lateral neocortical regions. These findings are consonant with postmortem assessments because the five laminar patterns of neurodegeneration are established early and, therefore, may contribute to glucose hypometabolism. Also, posterior cortical atrophy with Bálint syndrome-like signs suggest a more severe neurofibrillary and neuron degeneration in PCC than in lateral neocortices and imply an earlier involvement of PCC (40, 41, 86, 90). Very early glucose hypometabolism and early neuropathological subtypes cast a new perspective on the contributions of PCC to brain function and its role in AD pathology.

It has been known for some time that PCC is involved in visuospatial functions. Single neurons in monkey PCC code for the position of the eye in the orbit and large visual field patterns (66, 67). Lesions in this region impair spatial memory (61) and spatial tasks alter glucose metabolism in the retrosplenial areas (54). Finally, Hirono *et al.* (34) reported a correlation between glucose hypometabolism in right PCC and spatial disorientation in AD. Thus, functional impairments in visuospatial processing in AD may be due to functional disruption of PCC.

Since the first report classifying AD cases according to laminar patterns of neurodegeneration, it has been incorrectly suggested that ST0 represents the earliest state of neuropathology in PCC for all cases. This is not the premise of subtype analysis nor is it compatible with the present findings. The 7% of the cases with normal neuron counts have a full range of disease durations, not just 1–3 years as would be required if this were a precursor for all other subtypes. The presence of intact neuron counts in definite AD is not unique to PCC and has been observed in prefrontal cortex (77) and in other studies of cingulate cortex (12, 51, 89). The neuropathological subtypes do not proceed from ST0 to STIIIab to STIV–V to STII–V to STSevere. These are qualitatively independent subtypes. Finally, the integrity of neurons in these cases does not indicate that cingulate cortex is unimpaired because they have elevated M_2 binding in layers V and VI (82) and reduced $GABA_A$ binding in layer I (83). Since these are clinically diagnosed cases, the extent to which the clinical syndrome depends on neurodegeneration is accounted for by other neocortices. Thus, multivariate models of neocortical damage will require assessments of each cortical lobe and the subtypes hypothesis suggests that laminar patterns of neurodegeneration are an important variable not limited to PCC. The many examples of multifocal atrophy in frontotemporal and parietooccipital cortices and AD cases with a normal density of neurons in prefrontal cortex (86) suggest that models of AD subtypes require a broad definition of neuron loss.

Valenstein *et al.* (78) reported a case of "retrosplenial amnesia" with profound disruption of anterograde and retrograde memory. There is a long history of studies implicating PCC in memory in experimental species (reviews: 84, 85) and functional imaging in human (28). Although medial temporal areas have a role in memory, early impairments in PCC may be responsible for some of these functions in AD. Furthermore, there may be a pivotal integrative role for PCC that joins visuospatial and memory functions in a way that does not occur in other regions. Disruption of unique integrative functions in PCC may account for the earliest impairments in brain function in AD and the hypothesis of nodal visuospatial and memory processing in PCC implies that disruption of neuronal function in this region may result in nonlinear functional impairments.

Independence of Neuropathological Subtypes

One of the arguments for subtypes is that statistical subgroups represent etiologically unique and, therefore, independent neuropathological subtypes. Pivotal to this argument are the qualitatively different laminar patterns in neurodegeneration and a full range of disease durations for each subtype. Table 3 summarizes the features of each subtype. Although differences between STII–V and STSevere could be quantitative, almost every measure shown in Table 3, except disease duration, distinguishes between them including age at onset, amyloid deposition, laminar patterns of tau-ir NFT, and proportion of $\epsilon 4$ homozygotes. Neurodegeneration in STII–V, therefore, represents a fundamentally different process than that in STSevere. Another possible interrelation is between ST0 and STIIIab, since the former could progress into the latter or into STIV–V or STII–V. This is not true, however, because ST0 can have a duration of from 1 to 10 years and the subtypes are established around the time of clinically significant disease. The ST0 has about half the number of SP in STIIIab and the age at onset is about the same for all subtypes except STSevere. Furthermore, eigenvector projections show subgrouping of each subtype, indicating that they do not overlap even with long-duration disease. Thus, the five PCC subtypes are independent entities under the umbrella designation of definite AD.

These studies of PCC support the hypothesis of unique etiologies because each of the laminar patterns likely requires a different mechanism. Since the deposition of SP and NFT occurred in all subtypes at an

approximately equal level except in STSevere, differences in these markers do not reflect fundamentally different etiologies. Although the specific mechanisms by which neurons in each laminar profile are destroyed are not known, the different chemorachitectures of each cortical layer suggest associations that may lead to uncovering unique mechanisms for each subtype. Two extremes reflected in the subtypes suggest unique mechanisms (86). In STIIIab and STIV–V, a selective mechanism is required to destroy a small population of neurons. These layers have different densities of calcium-binding protein-positive neurons with layers II–IIIab having high levels of calretinin and deeper layers having fewer neurons expressing this protein (65). Since calretinin and calbindin expression is stable in interneurons in AD (35, 39), the low level of a calcium-binding proteins in deeper layers could make them selectively vulnerable to calcium-mediated events such as glutamate neurotoxicity. In contrast, STII–V and STSevere have significant neurodegeneration in all layers. Nitric oxide synthase is in a small number of widely distributed cortical interneurons, it mediates glutamate neurotoxicity (17), and altered activity in this enzyme could lead to "widespread neurotoxicity" in the cortex (16).

ApoE Genotype is not Related to Specific Patterns of Neurodegeneration

An assessment of the total relative number of neurons in frontal, parietal, and medial temporal cortices could not detect an ApoE genotype influence (48). Individuals homozygous for the ApoE $\epsilon 4$ allele have high densities of SP (75) and this is true for PCC; however, the broad distribution of SP in AD neocortex and lack of a relationship to laminar patterns of neuron losses suggests that ApoE genotype is secondary to events driving neurodegeneration. SP appear early in AD (2), their density is unrelated to the distribution of neocortical neurodegeneration (77, 89), and there are instances of many SP in elderly individuals with preserved mental status (9, 15, 36, 44, 75, 76). Thus, mechanisms like ApoE genotype that modulate SP density are unlikely to trigger neurodegeneration. The present study used four strategies to assess ApoE genotype and neurodegeneration and none showed a unique laminar pathology associated with a particular genotype. The STSevere had the greatest proportion of $\epsilon 4$ homozygotes, greatest neuron loss, and most SP and it alone may be influenced by this genotype. The within-subtype analysis of genotype failed to show that a severe loss of neurons, even in STSevere, is due to the prevalence of $\epsilon 4$ homozygotes. The ApoE $\epsilon 4$ risk is a general one that may interact with other genetic defects to influence amyloid deposition yet does not directly induce neurodegeneration.

NFT Are a Weak Measure of Neocortical Neurodegeneration

The present observations suggest that tau immunohistochemistry is helpful for defining the course of AD within a subtype but, given the wide range of tau-ir NFT densities and their variable laminar positions, they cannot be used as a marker for a single subtype. In PCC, a high density of tau-ir NFT in layers II and/or IIIab suggest a late-stage of disease progression. This pattern of NFT formation is opposite to that in entorhinal cortex where the earliest NFT occur in layer II (10, 25, 33, 36, 81). Also, entorhinal NFT in layer II are proportional to neurodegeneration (25) which is not true for PCC.

In PCC thioflavine S-stained NFT are light and they are not significantly related to neurodegeneration or subtype. The present study assessed tau-ir NFT in layers III and V where they tend to be most dense and even here there appeared to be a loss of eight neurons for each NFT. Finally, in late-stage cases (i.e., durations over 11 years), there were fewer NFT in layer V than in short-duration cases. If it is true that some NFT may be removed from the neuropil, their density is an even weaker measure of neurodegeneration.

Rationale for Atrophy Correction

Since an earlier study of PCC (89), the concern has been raised that an atrophy correction would produce a more accurate assessment of neuron losses. The present study shows that atrophy correction can normalize the density of neurons in layers that have both severe atrophy and severe neurodegeneration cancelling profound changes in laminar architecture. In retrospect, the rationale for atrophy correction in neocortex may be flawed because atrophy is not uniformly explained by the loss of perikarya. First, in a disease where neurons degenerate in layers III and V, the contributions of dendritic loss is not uniform. Layer V pyramidal neurons contribute apical dendrites to layer III but layer III neurons do not significantly contribute dendrites to layer V. This should result in greater shrinkage of layer III associated with dendrites. Second, the deep cortical layers have a greater proportion of myelinated axons passing through the neuropil than do layers II–III. This supporting myelin architecture may render the deep layers less susceptable to shrinkage than the superficial layers. Third, termination of corticocortical connections is mainly in the superficial layers and loss of these terminals should cause a differential reduction in neuropil in the external layers. Until a stereological method is devised to estimate total neurons in each layer of PCC in AD, atrophy correction is contraindicated.

Overview

The demonstration of five neuropathological subtypes within AD suggests strategies for studying multiple AD etiologies including focussing on neurodegeneration rather than SP and NFT. Assessment of the unique chemoarchitectural features and connections of neurons in different cortical layers should eventually lead to an understanding of the mechanisms underlying AD pathogenesis. The five patterns observed in PCC may not be limited to this region, but extensive studies of other areas with a similar statistical strategy will be needed. Also, subtypes based on laminar patterns of neurodegeneration may encompass cases with multifocal cortical atrophy that often have unique clinical presentations such as posterior cortical atrophy with Bálint syndrome-like symptoms. Finally, global models of AD that invoke a single mechanism such as the cholinergic and ApoE genotype hypotheses cannot account for multifocal mechanisms of neurodegeneration in the cerebral cortex. The present strategy for assessing neurodegeneration with multivariate models can be used to characterize etiopathologies that subserve multiple clinical endpoints.

REFERENCES

1. Armstrong, R. A., L. Wood, D. Myers, and C. U. M. Smith. 1996. The use of multivariate methods in the identification of subtypes of Alzheimer's disease: A comparison of principal components and cluster analysis. *Dementia* **7:** 215–220.
2. Arriagada, P. V., J. H. Growdon, E. T. Hedley-Whyte, and B. T. Hyman. 1992. Neurofibrillary tangles but not senile plaques parallel duration and severity of Alzheimer's disease. *Neurology* **42:** 631–639.
3. Bálint, R. 1909. Seelenlähmung des "Schauens," optische Ataxie, räumliche Störung der Aufmerksamkeit. *Mschr. Psychiatr. Neurol.* **25:** 51–81.
4. Bennett, D. A., E. J. Cochran, C. B. Saper, J. B. Leverenz, D. W. Gilley, and R. S. Wilson. 1993. Pathological changes in frontal cortex from biopsy to autopsy in Alzheimer's disease. *Neurobiol. Aging* **14:** 589–596.
5. Benson, D. F., R. J. Davis, and D. B. Snyder. 1988. Posterior cortical atrophy. *Arch. Neurol.* **45:** 789–793.
6. Bird, T. D., S. Stranaham, S. M. Sumi, and M. Radkind. 1983. Alzheimer's disease: Choline acetyltransferase activity in brain tissue from clinical and pathological subtypes. *Ann. Neurol.* **14:** 284–293.
7. Blacker, D., J. L. Haines, L. Rodes, R. H. Terwedow, L. E. Harrell, R. T. Perry, S. S. Bassett, D. Meyers, M. S. Albert, and R. Tanzi. 1997. ApoE-4 and age at onset of Alzheimer's disease: The NIMH genetics initiative. *Neurology* **48:** 139–147.
8. Bondareff, W., C. Q. Mountjoy, and M. Roth. 1982. Loss of neurons of origin of the adrenergic projection to cerebral cortex (nucleus locus ceruleus) in senile dementia. *Neurology* **32:** 164–168.
9. Bouras, C., P. R. Hof, P. Giannakopoulos, J. P. Michael, and J. H. Morrisson. 1994. Regional distribution of neurofibrillary tangles and senile plaques in the cerebral cortex of elderly individuals: A quantitative evaluation of a one-year autopsy population from a geriatric hospital. *Cereb. Cortex* **4:** 138–150.
10. Braak, H., and E. Braak. 1991. Neuropathological stageing of Alzheimer-related changes. *Acta Neuropathol.* **82:** 239–259.
11. Braak, H., and E. Braak. 1993. Alzheimer neuropathology and limbic circuits. In *Neurobiology of Cingulate Cortex and Limbic Thalamus* (B. A. Vogt and M. Gabriel, Eds.), pp. 606–626. Birkhäuser, Boston.
12. Brun, A., and E. Englund. 1981. Regional pattern of degeneration in Alzheimer's disease: Neuronal loss and histopathological grading. *Histopathology* **5:** 549–564.
13. Buée-Scherrer, V., O. Conamines, C. Mourton-Gilles, R. Jakes, M. Goedert, B. Pau, and A. Delacourte. 1996. AD2, a phosphorylation-dependent monoclonal antibody directed against tau proteins found in Alzheimer's disease. *Mol. Brain Res.* **39:** 79–88.
14. Chui, H. C., E. L. Tneg, V. W. Henderson, and A. C. Moy. 1985. Clinical subtypes of dementia of the Alzheimer type. *Neurology* **35:** 1544–1550.
15. Crystal, H., D. Dickson, P. Fuld, D. Masur, R. Scott, M. Mehler, J. Masdeu, C. Kawas, M. Aronson, and L. Wolfson. 1988. Clinico-pathologic studies in dementia: Nondemented subjects with pathologically confirmed Alzheimer's disease. *Neurology* **38:** 1682–1687.
16. Dawson, V. L., D. S. Bredt, D. S. Fotuhi, P. M. Hwang, and S. H. Snyder. 1991. Nitric oxide synthase and neuronal NADPH-diaphorase are identical in brain and peripheral tissues. *Proc. Natl. Acad. Sci. USA* **88:** 7797–7801.
17. Dawson, V. L., T. M. Dawson, E. D. London, D. S. Bredt, and S. H. Snyder. 1991. Nitric oxide mediates glutamate neurotoxicity in primary cortical cultures. *Proc. Natl. Acad. Sci. USA* **88:** 6368–6371.
18. Filley, C. M., J. Kelly, and R. K. Heaton. 1986. Neuropsychiatric features of early- and late-onset Alzheimer's disease. *Arch. Neurol.* **43:** 574–576.
19. Fisher, N. J., B. P. Rourke, L. Bieliauskas, B. Giordani, S. Berent, and N. Foster. 1996. Neuropsychological subgroups of patients with Alzheimer's disease. *J. Clin. Exp. Neuropsychol.* **18:** 349–370.
20. Fletcher, W. A. 1994. Ophthalmological aspects of Alzheimer's disease. *Curr. Opin. Ophthalmol.* **5:** 38–44.
21. Fletcher, W. A., and J. A. Sharpe. 1988. Smooth pursuit dysfunction in Alzheimer's disease. *Neurology* **38:** 272–277.
22. Foster, N. L., T. N. Chase, P. Fedio, N. J. Petronsas, R. A. Brooks, and G. DiChiro. 1983. Alzheimer's disease: Focal cortical changes shown by positron emission tomography. *Neurology* **33:** 961–965.
23. Furey-Kurkjian, M. L., P. Pietriyni, N. R. Graff-Radford, G. E. Alexander, U. Freo, J. Szczepanik, and M. B. Schapiro. 1996. Visual variant of Alzheimer's disease: Distinctive neuropsychological features. *Neuropsychology* **10:** 294–300.
24. Gioia, L., L. J. Vogt, W. M. Freeman, B. A. Vogt, and K. E. Vrana. 1998. PCR-based apolipoprotein E genotype analysis from archival fixed brain. *J. Neurosci. Methods* **80:** 209–214.
25. Gómez-Isla, T., J. L. Price, D. W. McKeel Jr., J. C. Morris, J. H. Growdon, and B. T. Hyman. 1996. Profound loss of layer II entorhinal cortex neurons occurs in very mild Alzheimer's disease. *J. Neurosci.* **16:** 4491–4500.
26. Gouras, G. K., N. R. Relkin, D. Sweeney, D. G. Munoz, I. R. Mackenzie, and S. Gandy. 1997. Increased apolipoprotein E $\epsilon 4$ in epilepsy with senile plaques. *Ann. Neurol.* **41:** 402–404.
27. Grady, C. L., J. V. Haxby, M. B. Shapiro, A. Kumar, M. J. Ball, L. Heston, and S. I. Rapoport. 1990. Subgroups in dementia of the Alzheimer type identified using positron emission tomography. *J. Neuropsychiatr.* **2:** 373–384.

28. Grasby, P. M., C. D. Frith, K. J. Friston, C. Bench, R. S. J. Frackowiak, and R. J. Dolan. 1993. Functional mapping of brain areas implicated in auditory-verbal memory function. *Brain* **116:** 1–20.

29. Grünthal, E. 1928. Hirnpathologischen Analyse der Alzheimerschen Krankheir. *Psychiat.-Neurol. Wschr.* **36:** 401–407.

30. Hardy, J. 1996. New insights into the genetics of Alzheimer's disease. *Ann. Med.* **28:** 255–258.

31. Haxby, J. V., R. Duara, C. L. Grady, N. R. Culter, and S. I. Rapoport. 1985. Relations between neuropsychological and cerebral metabolic asymmetries in early Alzheimer's disease. *J. Cereb. Blood Flow Metab.* **5:** 193–200.

32. Haxby, J. V., C. L. Grady, and E. Koss. 1988. Heterogeneous anterior-posterior metabolic patterns in dementia of the Alzheimer type. *Neurology* **38:** 1053–1063.

33. Hirano, A., and H. M. Zimmerman. 1962. Alzheimer's neurofibrillary changes; A topographic study. *Arch. Neurol.* **7:** 227–242.

34. Hirono, N., E. Mori, K. Ishii, Y. Ikejiri, T. Imamura, T. Shimomura, M. Hashimoto, H. Yamashita, and M. Sasaki. 1998. Hypofunction in the posterior cingulate gyrus correlates with disorientation for time and place in Alzheimer's disease. *J. Neurol. Neurosurg. Psychiatr.* **64:** 552–554.

35. Hof, P. R., N. Archin, A. P. Osmand, A. P. Dougherty, C. Wells, C. Bouras, and J. H. Morrison. 1993. Posterior cortical atrophy in Alzheimer's disease: Analysis of a new case and re-evaluation of a historical report. *Acta Neuropathol.* **86:** 215–223.

36. Hof, P. R., L. M. Bierer, D. P. Perl, A. Delacourte, L. Buée, C. Bouras, and J. H. Morrison. 1992. Evidence for early vulnerability of the medial and inferior aspects of the temporal lobe in an 82-year-old patient with preclinical signs of dementia. *Arch. Neurol.* **49:** 946–953.

37. Hof, P. R., C. Bouras, J. Constantinidis, and J. H. Morrison. 1989. Bálint's syndrome in Alzheimer's disease: Specific disruption of the occipitoparietal visual pathway. *Brain Res.* **493:** 368–375.

38. Hof, P. R., C. Bouras, J. Constantinidis, and J. H. Morrison. 1990. Selective disconnection of specific visual association pathways in cases of Alzheimer's disease presenting with Bálint's syndrome. *J. Neuropathol. Exp. Neurol.* **49:** 168–184.

39. Hof, P. R., and J. H. Morrison. 1991. Neocortical neuronal subpopulations labeled by a monoclonal antibody to calbindin exhibit differential vulnerability in Alzheimer's disease. *Exp. Neurol.* **111:** 293–301.

40. Hof, P. R., E. A. Nimchinsky, M. R. Celio, C. Bouras, and J. H. Morrison. 1993. Calretinin-immunoreactive neocortical interneurons are unaffected in Alzheimer's disease. *Neurosci. Lett.* **152:** 145–149.

41. Hof, P. R., B. A. Vogt, C. Bouras, and J. H. Morrison. 1997. Atypical form of Alzheimer's disease with prominent posterior cortical atrophy: A review of lesion distribution and circuit disconnection in cortical visual pathways. **Vision Res 37:** 3609–3625.

42. Hyman, B. T., K. Marzloff, and P. V. Arriagada. 1993. The lack of accumulation of senile plaques or amyloid burden in Alzheimer's disease suggests a dynamic balance between amyloid deposition and resolution. *J. Neuropathol. Exp. Neurol.* **52:** 594–600.

43. Hyman, B. T., H. L. West, T. Gomez-Isla, and S. Mui. 1995. Quantitative neuropathology in Alzheimer's disease: Neuronal loss in high-order association cortex paralleles dementia. In *Research Advances in Alzheimer's Disease and Relatedc Disorders* (K. Iqbal, J. A. Mortimer, and H. M. Wisniewski, eds.), pp. 453–460. Wiley, New York.

44. Katzman, R., R. Terry, R. DeTeresa, T. Brown, P. Davies, P. Fuld, X. Renbing, and A. Peck. 1988. Clinical, pathological, and neurochemical changes in dementia: A subgroup with preserved mental status and numerous neocortical plaques. *Ann. Neurol.* **23:** 138–144.

45. Khachaturian, Z. S. 1985. Diagnosis of Alzheimer's disease. *Arch. Neurol.* **42:** 1097–1105.

46. Kiyosawa, M., T. M. Bosley, J. Chawluk, D. Jamieson, N. J. Schatz, P. J. Savino, R. C. Sergott, M. Reivich, and A. Alavi. 1989. Alzheimer's disease with prominent visual symptoms. *Ophthalmology* **96:** 1077–1086.

47. Kurylo, D. D., S. Corkin, R. P. Dolan, J. F. Rizzo III, S. W. Parker, and J. H. Growdon. 1994. Broad-band visual capacities are not selectively impaired in Alzheimer's disease. *Neurobiol. Aging* **15:** 305–311.

48. Lippa, C. F., A. M. Saunders, T. W. Smith, J. M. Swearer, D. A. Drachman, B. Ghetti, L. Nee, D. Pulaski-Salo, D. Dickson, Y. Robitaille, C. Bergeron, B. Crain, M. D. Benson, M. Farlow, B. T. Hyman, P. St. George-Hyslop, A. D. Roses, and D. A. Pollen. 1996. Familial and sporadic Alzheimer's disease: Neuropathology cannot exclude a final common pathway. *Neurology* **46:** 406–412.

49. Lippa, C. F., T. W. Smith, and J. M. Swearer. 1994. Alzheimer's disease and Lewy body disease: A comparative clinicopathological study. *Ann. Neurol.* **35:** 81–88.

50. Mann, D. M. A., B. Marcyniuk, P. O. Yates, D. Neary, and J. S. Snowden. 1988. The progression of the pathological changes of Alzheimer's disease in frontal and temporal neocortex examined at biopsy and at autopsy. *Neuropathol. Appl. Neurobiol.* **14:** 177–195.

51. Mann, D. M. A., P. O. Yates, and B. Marcyniuk. 1985. Some morphometric observations on the cerebral cortex in presenile Alzheimer's disease and Down's syndrome in middle age. *J. Neurol. Sci.* **69:** 139–159.

52. Martin, A. 1987. Representation of semantic and spatial knowledge in Alzheimer's patients: Implications for models of preserved learning and amnesia. *J. Clin. Exp. Neuropsychol.* **9:** 191–224.

53. Martin, A. 1990. Neuropsychology of Alzheimer's disease: The case for subgroups. In *Modular Deficits in Alzheimer-type Dementia* (M. Schwartz, Ed.), pp. 145–175. MIT Press, Cambridge, MA.

54. Matsunami, K. I., T. Kawashima, and H. Satake. 1989. Mode of [^{14}C]2-deoxy-D-glucose uptake into retrosplenial cortex and other memory-related structures of the monkey during a delayed response. *Brain Res. Bull.* **22:** 829–838.

55. McKeith, I. G., D. Galasko, K. Kosaka, *et al.* 1996. Consensus guidelines for the clinical and pathologic diagnosis of dementia with Lewy bodies. *Neurology* **47:** 1113–1124.

56. Mirra, S. S., A. Heyman, and D. McKeel. 1991. The consortium to establish a registry for Alzheimer's disease (CERAD). *Neurology* **41:** 479–486.

57. Minoshima, S., N. L. Foster, and D. E. Kuhl. 1994. Posterior cingulate cortex in Alzheimer's disease. *Lancet* **344:** 895.

58. Minoshima, S., B. Giordani, S. Berent, K. A. Frey, N. L. Foster, and D. E. Kuhl. 1997. Metabolic reduction in the posterior cingulate cortex in very early Alzheimer's disease. *Ann. Neurol.* **42:** 85–94.

59. Morel, F. 1945. Les aires striée, parastriée et péristriée dans les troubles de la fonction visuelle au cours de la maladie d'Alzheimer. *Confin. Neurol.* **6:** 238–242.

60. Mountjoy, C. Q., M. Roth, N. J. R. Evans, and H. M. Evans. 1983. Cortical neuronal counts in normal elderly controls and demented patients. *Neurobiol. Aging* **4:** 1–11.

61. Murray, E. A., M. Davidson, D. Gaffan, D. S. Olton, and S. Suomi. 1989. Effects of fornix transection and cingulate cortical ablation on spatial memory in rhesus monkeys. *Exp. Brain Res.* **74:** 173–186.

62. Nagy, Z., M. M. Esiri, K. A. Jobst, J. H. Morris, E. King, B. McDonal, S. Litchfield, A. Smith, L. Barnetson, and A. D. Smith. 1995. Relative roles of plaques and tangles in the dementia of Alzheimer's disease: Correlations using three sets of neuropathological criteria. *Dementia* **6:** 21–31.

63. Neary, D., and J. S. Snowden. 1987. Perceptuospatial disorder in Alzheimer's disease. *Semin. Ophthalmol.* **2:** 151–158.

64. Neary, D., J. S. Snowden, D. M. A. Mann, D. M. Bowen, N. R. Sims, B. Northen, P. O. Yates, and A. N. Davison. 1986. Alzheimer's disease: A correlative study. *J. Neurol. Neurosurg. Psych.* **49:** 229–237.

65. Nimchinsky, E. A., B. A. Vogt, J. H. Morrison, and P. R. Hof. 1997. Neurofilament and calcium-binding proteins in the human cingulate cortex. *J. Comp. Neurol.* **384:** 597–620.

66. Olson, C. R., S. Y. Musil, and M. E. Goldberg. 1993. Posterior cingulate cortex and visuospatial cognition: Properties of single neurons in the behaving monkey. In *Neurobiology of Cingulate Cortex and Limbic Thalamus* (B. A. Vogt and M. Gabriel, Eds.), pp. 366–380. Birkhäuser, Boston.

67. Olson, C. R., S. Y. Musil, and M. E. Goldberg. 1996. Single neurons in posterior cingulate cortex of behaving macaque: Eye movement signals. *J. Neurophysiol.* **76:** 3285–3300.

68. Paik, Y. K., D. J. Chang, C. A. Reardon, G. E. Davies, R. W. Mahley, and J. M. Taylor. 1985. Nucleotide sequence and structure of the human apolipoprotein E gene. *Proc. Natl. Acad. Sci. USA* **82:** 3445–3449.

69. Pearson, R. C. A., M. M. Esiri, R. W. Hiorns, G. K. Wilcock, and T. P. S. Powell. 1985. Anatomical correlates of the distribution of the pathological changes in the neocortex in Alzheimer disease. *Proc. Natl. Acad. Sci. USA* **82:** 4531–4534.

70. Pietrini, P., M. L. Furey, N. Graff-Radford, U. Freo, G. E. Alexander, C. L. Grady, A. Dani, M. J. Mentis, and M. B. Shapiro. 1996. Preferential metabolic involvement of visual cortical areas in a subtype of Alzheimer's disease: Clinical implications. *Am. J. Psych.* **153:** 1261–1268.

71. Procter, A. W., S. L. Lowe, A. M. Palmer, P. T. Francis, M. M. Esiri, G. C. Stratmann, A. Najlerahim, A. J. Patel, A. Hunt, and D. M. Bowen. 1988. Topographical distribution of neurochemical changes in Alzheimer's disease. *J. Neurol. Sci.* **84:** 125–140.

72. Rossor, M. N., N. J. Garrett, A. L. Johnson, C. Q. Mountjoy, R. Roth, and L. L. Iversen. 1982. A post-mortem study of cholinergic and GABA systems in senile dementia. *Brain* **105:** 313–330.

73. Rossor, M. N., L. L. Iversen, G. P. Reynolds, C. Q. Mountjoy, and M. Roth. 1984. Neurochemical characteristics of early and late onset types of Alzheimer's disease. *Br. Med. J.* **288:** 961–964.

74. Schmechel, D. E., A. M. Saunders, W. J. Strittmater, B. J. Crain, S. H. Joo, M. A. Pericak-Vance, D. Goldgaber, and A. D. Roses. 1993. Increased amyloid β-peptide deposition in cerebral cortex as a consequence of apolipoprotein E genotype in late-onset Alzheimer disease. *Proc. Natl. Acad. Sci. USA* **90:** 9649–9653.

75. Sparks, D. L., J. C. III, Hunsaker, S. W. Scheff, R. J. Kryscio, J. L. Hensen, and W. R. Markesbery. 1990. Cortical senile plaques in coronary artery disease, aging and Alzheimer's disease. *Neurobiol. Aging* **11:** 601–607.

76. Sparks, D. L., S. W. Scheff, H. Liu, T. Landers, F. Danner, C. M. Coyne, and J. C. Hunsker III. 1996. Increased density of senile plaques, but not neurofibrillary tangles in non-demented individuals with the apolipoprotein E4 allele: Comparison to confirmed Alzheimer's disease patients. *J. Neurol. Sci.* **138:** 97–104.

77. Terry, R. D., A. Peck, R. DeTeresa, R. Schechter, and D. S. Horoupian. 1981. Some morphometric aspects of the brain in senile dementia of the Alzheimer type. *Ann. Neurol.* **10:** 184–192.

78. Valenstein, E., D. Bowers, M. Verfaellie, K. M. Heilman, A. Day, and R. T. Watson. 1987. Retrosplenial amnesia. *Brain* **110:** 1631–1646.

79. Van Hoesen, G. W., B. T. Hyman, and A. R. Damasio. 1991. Entorhinal cortex pathology in Alzheimer's disease. *Hippocampus* **1:** 1–8.

80. Vickers, J. C., B. M. Riederer, R. A. Marugg, V. Buée-Scherrer, L. Buée, A. Delacourte, and J. H. Morrison. 1994. Alterations in neurofilament protein immunoreactivity in human hippocampal neurons related to normal aging and Alzheimer's disease. *Neuroscience* **62:** 1–13.

81. Victoroff, J., W. Ross, D. F. Benson, M. A. Verity, and H. V. Vinters. 1994. Posterior cortical atrophy—Neuropathologic correlations. *Arch. Neurol.* **51:** 269–274.

82. Vogt, B. A., P. B. Crino, and L. J. Vogt. 1992. Reorganization of cingulate cortex in Alzheimer's disease: Neuron loss, neuritic plaques, and muscarinic receptor binding. *Cereb. Cortex* **2:** 526–535.

83. Vogt, B. A., P. B. Crino, and L. Volicer. 1991. Laminar alterations in gamma-aminobutyric $acid_A$, muscarinic and beta adrenoceptors and neuron degeneration in cingulate cortex in Alzheimer's disease. *J. Neurochem.* **57:** 282–290.

84. Vogt, B. A., D. M. Finch, and C. R. Olson. 1992. Functional heterogeneity in cingulate cortex: The anterior executive and posterior evaluative regions. *Cereb. Cortex* **2:** 435–443.

85. Vogt, B. A., and M. Gabriel. 1993. *Neurobiology of Cingulate Cortex and Limbic Thalamus.* Birkhäuser, Boston.

86. Vogt, B. A., A. Martin, K. E. Vrana, J. R. Absher, L. J. Vogt, and P. R. Hof. 1998. Multifocal cortical neurodegeneration in Alzheimer's disease. In *Cerebral Cortex* (A. Peters and J. H. Morrison, Eds.). Plenum Press: New York.

87. Vogt, B. A., E. A. Nimchinsky, L. J. Vogt, and P. R. Hof. 1995. Human cingulate cortex: Surface features, flat maps, and cytoarchitecture. *J. Comp. Neurol.* **359:** 490–506.

88. Vogt, B. A., and D. N. Pandya. 1987. Cingulate cortex of the rhesus monkey. II. Cortical afferents. *J. Comp. Neurol.* **262:** 271–289.

89. Vogt, B. A., G. W. Van Hoesen, and L. J. Vogt. 1990. Laminar distribution of neuron degeneration in posterior cingulate cortex in Alzheimer's disease. *Acta Neuropathol.* **80:** 581–589.

90. Vogt, B. A., L. J. Vogt, E. A. Nimchinsky, and P. R. Hof. 1997. Primate cingulate cortex chemoarchitecture and its disruption in Alzheimer's disease. In *Handbook of Chemical Neuroanatomy. Vol. 13. The Primate Nervous System, Part 1.* (F. E. Bloom, A. Björklund, and T. Hökfelt, Eds.), Part 1, pp. 455–528. Elsevier, Amsterdam.

91. Yankner, B. A. 1995. Mechanisms of neuronal degeneration in Alzheimer's disease. *Neuron* **16:** 921–932.